Investigation of the Impact of Slider Mass Stiffness on the Behavior of the Variable Inertia Rotational Mechanism for Structural Vibration Mitigation

Anika T. Sarkar[1], and Nicholas E. Wierschem[1]

[1]Department of Civil and Environmental Engineering
Tickle College of Engineering

University of Tennessee, Knoxville, TN 37996

ABSTRACT
Structural control devices can help to mitigate the response and subsequent damage to structures that result from dynamic loads, such as earthquakes and wind loads. Rotational inertial mechanisms offer a promising avenue for achieving this goal by providing significant mass effects without the need for large physical masses. Among these mechanisms, the variable inertia rotational mechanism (VIRM) is a nonlinear control device with adjustable rotational inertia and thus produces modifiable mass effects, achieved by incorporating slider masses inside the device's flywheel. While previous research on the VIRM has predominantly focused on active or semi-active control systems, the passive implementation of VIRM and its efficacy in vibration mitigation remains relatively unexplored. As a result, the effects of the device parameters, most prominently slider stiffness, and the impact of these parameters on the device's ability to reduce response under random excitation are uncertain. This paper addresses these gaps in knowledge through a numerical study considering a single-degree-of-freedom primary structure. The study aims to investigate the different stiffness characteristics of the VIRM, including modeled properties of the stiffness element attached to the slider masses, on the natural frequency shifts and response mitigation. The natural frequency and response measures are evaluated by estimating the system's instantaneous frequency and an H_2-based measure. The results of this study highlight the ability of VIRM to shift natural frequencies and reduce response in structures subjected to random excitation and will encourage the further study of these innovative devices.

Keywords: Nonlinear, Inerter, Variable Inertia, Stiffness, Passive Control

INTRODUCTION

Rotational inertia mechanisms (RIMs), most commonly the inerters, have been recently developed and the added effective mass these devices can provide has been utilized in a variety of ways to mitigate vibrations. RIMs are two terminal mechanical elements that can be physically realized with different means, such as a ball-screw assembly, rack and pinion assembly, and fluid-based mechanisms [1], [2]. Linear RIMs produce constant effective mass. Nonlinear RIMs can produce varying effective mass by utilizing geometric nonlinearities [3], [4], or by modifying its properties as a function of the device's response, such as the relative displacement or rotational velocity [5]–[8]. One such mechanism that has properties that alter based on the rotational velocity of the device's flywheel is called the variable inertia rotational mechanism (VIRM).

A VIRM can be developed by mounting multiple symmetrically spaced slider masses inside the device's flywheel using springs and guides (see Figure 1b). A ball-screw assembly connects the flywheel to the structure, causing the flywheel to rotate when there is relative motion between the device's terminals. The flywheel's rotational velocity $\left(\dot{\theta}\right)$ is proportional to the relative velocity $\left(\dot{u}\right)$ between the connection terminals of the VIRM. The proportionality constant $\left(\alpha\right)$ is $2\pi/\rho$ for a ball-screw, where ρ is the ball screw's lead. The rotation of the flywheel causes the slider masses to move within the guide and larger flywheel rotational velocities result in the slider masses moving further out radially. These movements result in changes in the rotational inertia of the flywheel and, thus, changes in the mass effects the VIRM provides.

The majority of the previous VIRM research has investigated its effectiveness in energy storage, vibration control and stability of attached machinery [5], [7], [9], [10]. Although previous studies have explored parametric variations in VIRM slider mass stiffness to assess system performance, the slider stiffnesses considered were identical in the assembly. There is a gap in understanding how introducing dissimilarities in the stiffness elements connecting the slider masses in the VIRM flywheel could affect system dynamics and the system's capacity for response mitigation. Additionally, the performance of the structure is typically analyzed using harmonic or impulse loading conditions, thus its behavior under random excitation scenarios remains uncertain. Consequently, critical knowledge gaps exist regarding the impact of dissimilar slider stiffnesses of a VIRM on a system's natural frequency and its ability to mitigate responses when exposed to random vibration.

This work aims to fill these gaps by numerically investigating the natural frequency shifts of a VIRM attached to a single-degree-of-freedom (SDOF) primary system subjected to a random excitation force (see Figure 1a). Additionally, this work explores the impact of dissimilar slider stiffness properties on the system behavior and response attenuation performance. The effect of load amplitude changes on the frequency shifts and response reduction are also investigated. Comparisons in this study are made with the behavior and performance of the same primary system with an attached VIRM with sliders with identical stiffness.

The organization of this paper is as follows. In the next section, the mathematical model of a VIRM installed in a single-degree-of-freedom primary system is presented. Additionally, system and VIRM parameters and loading properties are described. The numerical analyses result section describes the simulation results and the last section concludes with a review of the findings of this work.

MATHEMATICAL MODEL OF THE SYSTEM

In this study, a VIRM is considered in which four slider mass-spring-dampers are symmetrically placed on a circular flywheel, as illustrated in Figure 1b. The springs are modeled to have a trilinear elastic force-displacement relationship, with a soft central stiffness zone, k_{sd}, and two stiffer and equal penalty stiffness zones, k_p (see Figure 1c). When the slider masses reach a lower bound (R_{lbc}) or upper bound contact point (R_{ubc}) along the guide, the penalty stiffness zone engages and helps to constrain the slider mass movement. The focus of this work is to evaluate the impact of dissimilar slider mass stiffnesses in a VIRM flywheel. In this work, dissimilar slider mass stiffnesses are considered such that two symmetrically spaced slider masses have a central stiffness $\left(k_{sd_1}\right)$ and the remaining set are twice as stiff $\left(k_{sd_2} = 2k_{sd_1}\right)$. Due to the presence of two slider stiffnesses in a VIRM, it is referred to as the dual stiffness VIRM (VIRM-DS). To compare the results of the VIRM-DS, two other VIRM configurations are investigated where all four sliders have identical stiffnesses, with low k_{sd_1} and high k_{sd_2} stiffnesses. These are referred to as low single stiffness VIRM (VIRM-SS (low)) and high single stiffness VIRM (VIRM-SS (high)), respectively. Unless otherwise noted, in each of these configurations, the penalty stiffness values are set at 200 times the soft stiffness: $k_{p_1} = 200k_{sd_1}, k_{p_2} = 200k_{sd_2}$ for the VIRM-DS and $k_p = 200k_{sd}$ for the VIRM-SS.

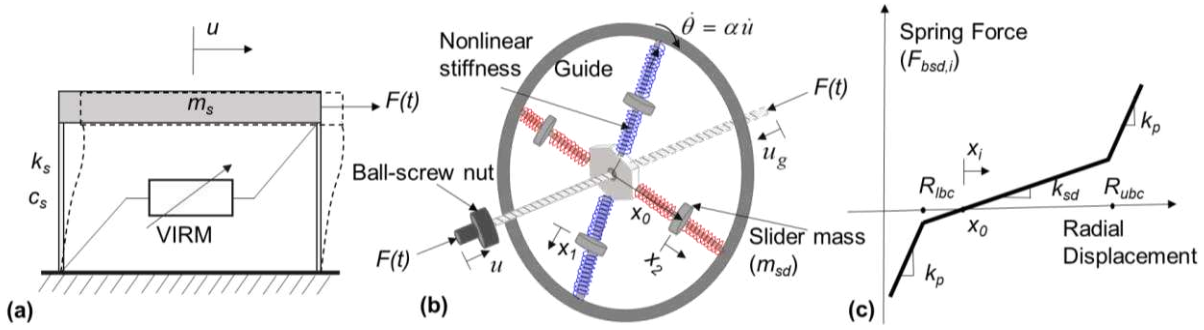

Figure 1. Schematic diagram of (a) primary system with VIRM, (b) VIRM-DS flywheel (blue denotes lower stiffness spring, k_{sd_1} and red denotes higher stiffness spring, k_{sd_2}), and (c) trilinear force versus radial position relationship for the slider mass springs

The displacement of the primary structure is u. The presence of two stiffnesses in the VIRM-DS add two additional degrees of freedom (DOF), x_1 and x_2, to the SDOF primary system compared to one additional DOF for the VIRM-SS, x. The equations of motion of the combined three DOF (VIRM-DS) system and two DOF (VIRM-SS) systems are shown in Eq. (1) and (2), respectively.

$$\begin{aligned} &m_s\ddot{u} + J\alpha^2\ddot{u} + nm_{sd}\alpha^2\dot{u}\left(x_1\dot{x}_1 + x_2\dot{x}_2\right) + \frac{n}{2}m_{sd}\alpha^2\ddot{u}\left({x_1}^2 + {x_2}^2\right) + c_s\dot{u} + k_s u = F(t) \\ &m_{sd}\ddot{x}_1 - m_{sd}x_1\alpha^2\dot{u}^2 + F_{bsd,1}\left(x_1\right) + c_{sd}\dot{x}_1 = 0 \\ &m_{sd}\ddot{x}_2 - m_{sd}x_2\alpha^2\dot{u}^2 + F_{bsd,2}\left(x_2\right) + c_{sd}\dot{x}_2 = 0 \end{aligned} \tag{1}$$

$$\begin{aligned} &m_s\ddot{u} + J\alpha^2\ddot{u} + 2nm_{sd}\alpha^2\dot{u}x\dot{x} + nm_{sd}\alpha^2\ddot{u}x^2 + c_s\dot{u} + k_s u = F(t) \\ &m_{sd}\ddot{x} - m_{sd}x\alpha^2\dot{u}^2 + F_{bsd}\left(x\right) + c_{sd}\dot{x} = 0 \end{aligned} \tag{2}$$

where, m_s, c_s, k_s, and $F(t)$ are the primary system's mass, damping, stiffness, and applied load, respectively; the VIRM properties of J, n, m_{sd}, and c_{sd}, are the static rotational inertia, number of sliders, slider mass, and slider damping, respectively. $F_{bsd,1}$, $F_{bsd,2}$ and F_{bsd} represent the restoring force of the VIRM-DS and VIRM-SS trilinear springs of the model, respectively. This trilinear spring relationship is presented by Figure 1c and can be defined as

$$\begin{aligned} &F_{bsd,i} = k_{sd_i}\left(R_{lbc} - x_0\right) + k_{p_i}\left(x_i - R_{lbc}\right),\ x_i < R_{lbc} \\ &F_{bsd,i} = k_{sd_i}\left(x_i - x_0\right),\ R_{lbc} \le x_i < R_{ubc} \\ &F_{bsd,i} = k_{sd_i}\left(R_{ubc} - x_0\right) + k_{p_i}\left(x_i - R_{ubc}\right),\ x_i \ge R_{ubc} \end{aligned} \tag{3}$$

In this study, numerical simulations are performed to investigate the response of the primary system with VIRM configurations when the structure is subjected to a band-limited white noise with a frequency range of 1 Hz to 8 Hz. In addition to investigating dissimilar slider stiffness configurations, differences resulting from changes in the overall stiffness of the slider mass springs are investigated in this study. The system and the RIM properties for these numerical simulations are shown in Table 1.

Table 1. Model parameter properties

Symbol	Description	Value
ω_s	Primary system's natural frequency (without RIM) (Hz)	5.8
n	Number of slider masses	4
k_{sd_1}	Slider soft low stiffness (N/m)	20, 50, 70, 100, 120
k_{sd_2}	Slider soft high stiffness (N/m)	40, 100, 140, 200, 240
m_{sd}	Slider mass (kg)	0.5
c_{sd}	Slider damping coefficient (Ns/m)	5
$\kappa = k_{p_i} / k_{sd_i}$	Slider penalty stiffness ratio	200
J	Flywheel static rotational inertia (kgm^2)	0.0026
ζ_s	Damping ratio of the primary system	2%
x_0	Initial position (m)	0.02
R_{ubc}	Radial position of the upper penalty spring (m)	0.095
R_{lbc}	Radial position of the lower penalty spring (m)	0.005
α	Proportionality constant between the relative velocity of the system and the angular velocity of the flywheel	200

NUMERICAL ANALYSES RESULTS

This section presents the results of numerical simulations of the primary system with various VIRM configurations, VIRM-DS, VIRM-SS (low), and VIRM-SS (high), and focuses on evaluating the effect of the VIRM slider stiffness on the behavior and response of the attached primary system. Various response measures are computed from the numerical analyses to assess the impact of the VIRM configuration on system behavior. The shift in natural frequencies is examined using wavelet transforms and the instantaneous frequency, which is a measure of the system's preferred vibration frequency. In a linear system, the instantaneous frequency remains constant, while in a nonlinear VIRM system, it can fluctuate with the response of the system. The impact of the VIRMs on vibration attenuation performance is measured using the H_2 norm analog, which quantifies the extent to which the system amplifies or attenuates energy under the applied load condition. To provide a basis of comparison, simulations are also performed with two versions of fixed inertia rotational mechanisms (FIRMs), where the VIRM slider masses are fixed at their initial position, x_0, or the upper bound contact point, R_{ubc}.

NATURAL FREQUENCY SHIFT

Figure 2 and Figure 3 show the displacement of the primary system and the resulting wavelet transform of the VIRM-DS, VIRM-SS (low) and VIRM-SS (high) configurations when the primary structure is subjected to white noise with low and high amplitudes, respectively. In addition to investigating the effect of dissimilar slider stiffness on the response and system behavior, low and high slider stiffnesses are investigated for all the VIRM configurations and the loading amplitudes. Wavelet plots help to visualize the time-dependent frequency components of the corresponding response time series, with dark-shaded regions in the contour plots representing higher amplitudes in system response at the associated time and frequency levels. Additionally, shading in the wavelet subplots are correlated; thus, the darkest shades in these wavelets are indicative of the highest amplitude for all the subplots. The Morlet wavelet is used as the mother wavelet in this study.

Figure 2(a) and (e) show that at low load amplitude, all the configurations have similar response amplitudes, regardless of the slider stiffnesses or dissimilarities in slider stiffness. It can also be observed from the wavelet results in Figure 2(b)-(d), (f)-(h) that there is a similar shading for all the VIRM configurations with the dominant frequencies between 5 Hz and 6 Hz, which indicate that the instantaneous frequency continuously shifts between that range. The limited shift in instantaneous frequency for low load amplitude is because the slider masses do not move significantly due to lower rotational velocity of the VIRM.

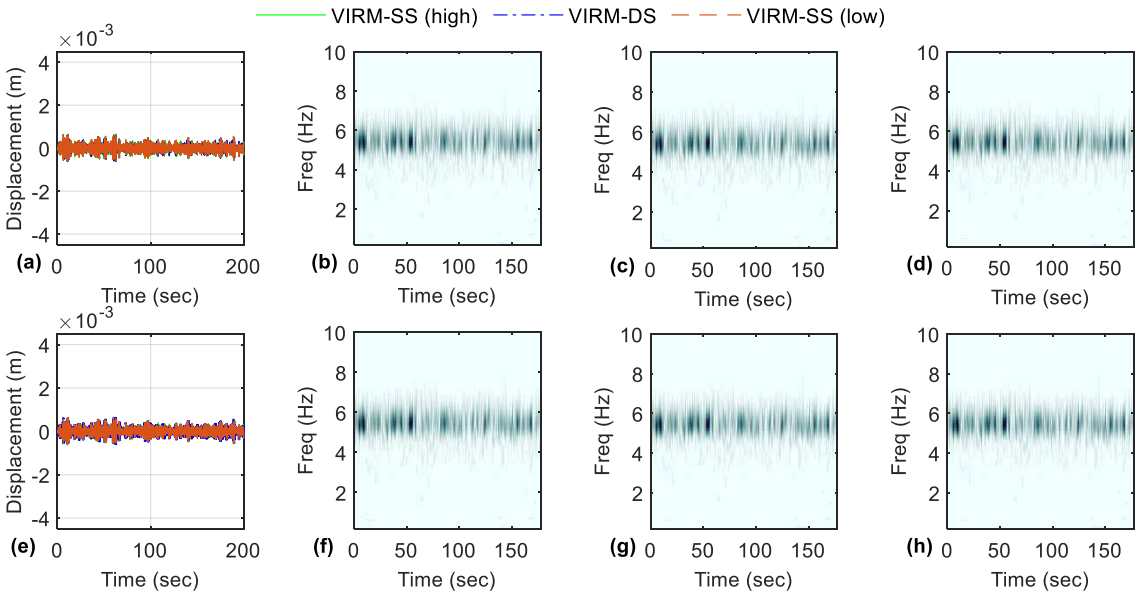

Figure 2. Displacement (a, e) and corresponding wavelets of the primary system connected to different VIRM configurations with low stiffness (a-d (k_{sd_1} =20 N/m) and high stiffness (e-h (k_{sd_1} =120 N/m)) for low white noise RMS amplitude of 15 ms^{-2}: (b, f) VIRM-SS (low), (c, g) VIRM-DS, (d, h) VIRM-SS (high)

The effect of slider stiffness on the system displacement and system behavior with the various VIRM configurations given a white noise with high amplitude is presented in Figure 3. Figure 3e shows that all configurations exhibit comparable responses, similar to the low load amplitude in Figure 2a and e. However, the variations are seen in the responses in Figure 3a, which feature systems with overall lower slider spring stiffnesses. The wavelets of the system with VIRM attachments, with k_{sd_1} =20 N/m, presented by Figure 3(b-d) show that the frequency content of the system's response varies much more than in the low load amplitude case: between 3 Hz and 6 Hz with the VIRM-SS (low) and between 3.5 Hz and 6 Hz with the VIRM-DS and VIRM -SS (high). The reason behind the lower natural frequency at the high load amplitude, compared to with the low load amplitude, is because at the high load amplitude, the slider masses experience higher centrifugal force, causing them to move further outward radially. It is also notable that the instants of noticeably lower frequency response for the VIRM-SS (low) configuration, at 60, 70, and 125 sec, corresponds to times near where the displacements of the primary system are the highest for the high loading case.

Moreover, the wavelets of Figure 3(b-d) show that that the system natural frequencies are relatively higher for the VIRM-DS than VIRM-SS (low) configuration. The higher natural frequency of the system attached with the VIRM-DS could be because two high slider stiffnesses in this configuration inhibits the further outward movement of those slider masses, overall increasing the natural frequency of the system. Figure 3 (f-h) present that at the same high load amplitude and for the slider stiffness of k_{sd_1} =120 N/m, the overall instantaneous frequency increases and ranges between 4.5 Hz and 6 Hz, similar to the low load amplitude. Furthermore, the increase in the slider stiffness results in a small increase in the displacement of the primary system.

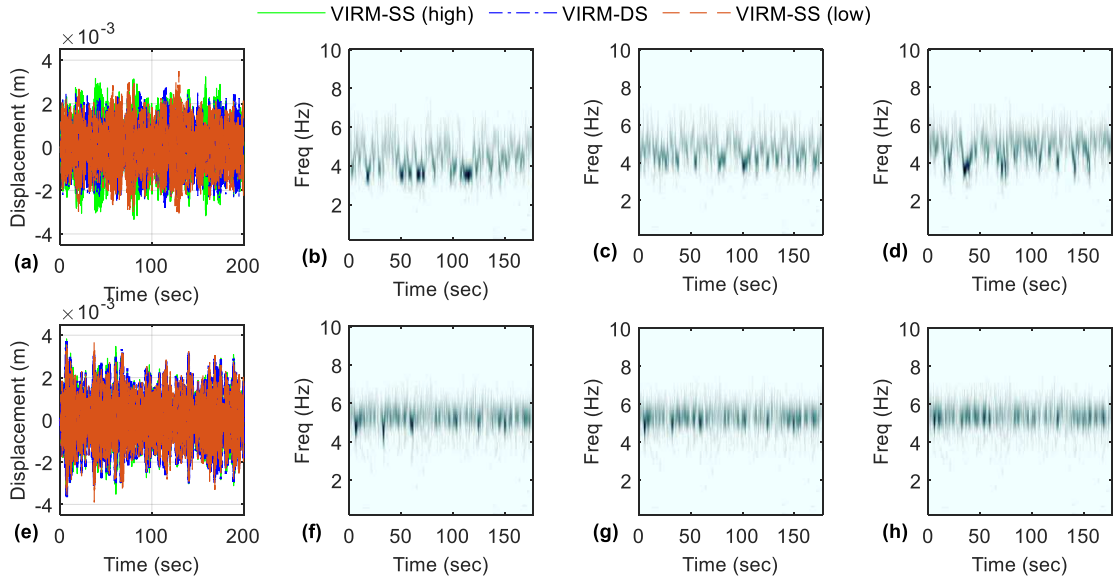

Figure 3. Displacement (a, e) and corresponding wavelets of the primary system connected to different VIRM configurations with low stiffness (a-d (k_{sd_1} =20 N/m) and high stiffness (e-h (k_{sd_1} =120 N/m)) for high white noise RMS amplitude of 116 ms^{-2}: (b, f) VIRM-SS (low), (c, g) VIRM-DS, (d, h) VIRM-SS (high)

The influence of the load amplitude and the slider stiffness on frequency shifts is investigated with the weighted average instantaneous frequency, ϖ_w, in Figure 4. To estimate the instantaneous frequency in this study, the nonlinear equations of motions are linearized by applying the small perturbation method and producing tangent mass and tangent stiffness matrices at each time step in the numerical simulation. Then, an eigenvalue analysis is performed to determine the instantaneous frequency at each time step. The instantaneous frequency of interest is isolated from these results by identifying the eigenvector where the DOF associated with the primary structure has the most significant contribution. Finally, using the total energy time history response as the weighting factor, a weighted average instantaneous frequency is computed.

Figure 4 shows that at low load amplitudes VIRM -DS, VIRM-SS (low), and VIRM-SS (high) have the same ϖ_w for all the slider stiffness values, similar to the FIRM with slider masses fixed at the initial position. As the load amplitude increases, ϖ_w decreases for all the VIRM configurations and stiffness values. However, the VIRM-SS (low) have lower ϖ_w compared to VIRM-DS and VIRM-SS (high). Moreover, as the slider stiffness increases, ϖ_w increases for all the configurations, which aligns with the results of the wavelets. The plots suggest that the presence of higher slider stiffness, whether in all of the sliders or in some of them, contribute to a higher weighted average instantaneous frequency as long as the amplitude of response is high enough. It is also observed that the FIRM with slider masses fixed at R_{ubc} have the lowest ϖ_w of all the configurations considered. The higher ϖ_w of the VIRMs than the FIRM (at R_{ubc}) could be because the average slider mass position of the VIRMs was mostly lower than R_{ubc}, adding a lower effective mass than the FIRM (at R_{ubc}).

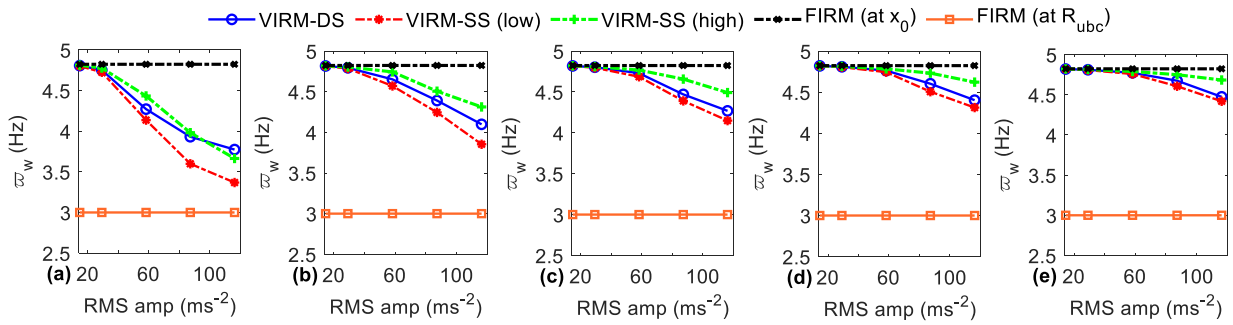

Figure 4. Effect on the weighted average instantaneous frequency of load amplitude and slider stiffness, k_{sd_1} : (a) 20 N/m, (b) 50 N/m, (c) 70 N/m, (d) 100 N/m, and (e) 120 N/m

RESPONSE MITIGATION

System performance can be measured using the H_2 norm analog measure, which is determined by taking the square of the area under the estimated transfer function of the system's response between the bounded frequency range of 1 Hz to 8 Hz. This frequency range is used to calculate this measure as it corresponds with the frequency range of the band-pass filtered white noise. Figure 5 presents the H_2 norm analog of the different VIRM configurations for different load amplitudes and slider stiffnesses. This figure shows that all the VIRM attachments have lower, or approximately the same, H_2 norm analog compared to the FIRM (at x_0). The figure also shows that at low loading amplitudes, the VIRM configurations have a slightly higher H_2 norm analog compared to the FIRM (at R_{ubc}). However, as the load amplitude increases, H_2 norm analog reduces significantly for the VIRM attached systems. Additionally, the VIRM-SS (low) is able to best reduce the response of the system in comparison to the other configurations. This lower response may be because of the larger continuous shifts in frequency and lager shift in overall frequency that are possible with the VIRM-SS (low). This figure also shows that higher slider stiffness, whether in all of the sliders or in some of them, decreases the response mitigation performance of the VIRM.

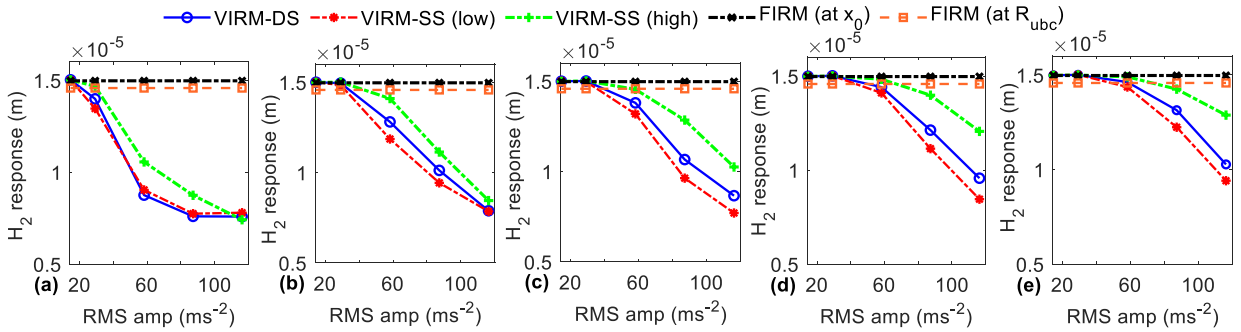

Figure 5. Effect on H_2 norm analog of load amplitude and slider stiffness, k_{sd_1} : (a) 20 N/m, (b) 50 N/m, (c) 70 N/m, (d) 100 N/m, and (e) 120 N/m, on the H_2 norm analog

While the results in Figure 5 may suggest that lower slider stiffness is always beneficial, this is not always true. For example, if the system with low a stiffness, k_{sd_1} =20 N/m, VIRM-DS is investigated at higher load amplitudes, it is observed that the system becomes unstable because the low slider stiffness masses are no longer restrained in the flywheel. This occurs because the effective outward force on the slider masses continuously exceeds the restoring forces working on these masses. In practical terms, this instability would result in a collision of the slider masses at its radial limit or necessitate large flywheel diameters.

PENALTY STIFFNESS VARIATIONS

To understand the effect of penalty stiffness on the system behavior and response, the system with VIRM-SS configurations is investigated further and is presented in Figure 6. The soft slider stiffnesses of 20 N/m and 70 N/m are considered for this analysis with various penalty stiffness ratios. Figure 6 (a) shows that for either soft slider stiffness, the ϖ_w increases as the penalty stiffness ratio increases. It is notable that at the softer slider stiffness of 20 N/m and κ=1, ϖ_w is significantly lower than at the other penalty stiffness ratios, as the penalty stiffness is no longer there to restrain the motion of the slider masses. The changes in response frequency content with different values are see in the wavelets in Figure 6 (c) and (d). While changes in penalty stiffness causes changes in the H_2 norm analog, the change is relatively small, except with softer slider stiffness of 20 N/m and κ=1, where large changes in H_2 norm analog are also observed.

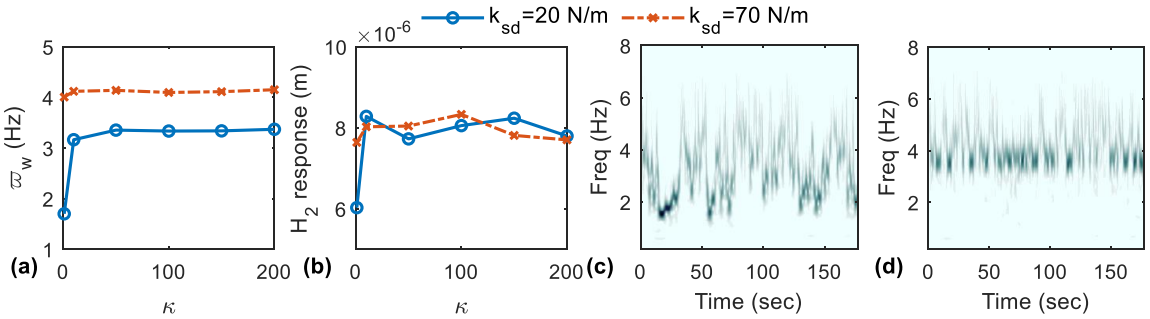

Figure 6. Effect of penalty stiffness ratio , κ , for a RMS band-limited white noise of 116 ms^{-2} of the VIRM-SS on the (a) system's weighted average instantaneous frequency, (b) H_2 response; (c) displacement wavelets of the system with VIRM-SS (k_{sd_1} =20 N/m, κ =1), and (d) displacement wavelets of the system with VIRM-SS (k_{sd_1} =20 N/m. κ =200),

CONCLUSIONS

The variable inertia rotational mechanism (VIRM) numerically investigated in this work includes the dissimilar slider stiffness configuration, which is denoted as dual stiffness VIRM (VIRM-DS) and features a stiffer spring connected to half of its slider masses. The results of the study show that the VIRM-DS generally has a slightly higher to similar weighted average instantaneous frequency than the low single stiffness VIRM (VIRM-SS (low)) across all the stiffnesses considered. However, in conditions of high loading amplitude and low stiffness, the VIRM-SS (low) displays notably lower weighted average instantaneous frequencies compare to the VIRM-DS. Furthermore, the study reveals that the VIRM-DS and different VIRM-SS configurations have similar response mitigation performance with the VIRM-SS (low) generally performing better. Overall, the paper suggests that the slider stiffness plays a significant role in influencing system dynamics and response mitigation. Furthermore, these results suggest that using dissimilar VIRM slider stiffnesses does not have any advantages over using the same slider stiffness. Future work should explore alternative stiffness models and penalty stiffness strategies in depth.

ACKNOWLEDGEMENTS
The research is funded by the National Science Foundation under Grant No. 1944513. The findings, opinions, recommendations, and conclusions in the paper are hose of the authors alone and do not reflect the views of others including the sponsors.

REFERENCES

[1] M. C. Smith, "Synthesis of mechanical networks: the inerter," *IEEE Trans. Autom. Control*, vol. 47, no. 10, pp. 1648–1662, Oct. 2002, doi: 10.1109/TAC.2002.803532.
[2] M. C. Smith, "Force-Controlling Hydraulic Device," US 2021/0199428 A1, Aug. 09, 2012
[3] F. de H. Moraes, M. Silveira, and P. J. P. Gonçalves, "On the dynamics of a vibration isolator with geometrically nonlinear inerter," *Nonlinear Dyn.*, vol. 93, no. 3, pp. 1325–1340, Aug. 2018, doi: 10.1007/s11071-018-4262-6.
[4] J. Yang, J. Z. Jiang, and S. A. Neild, "Dynamic analysis and performance evaluation of nonlinear inerter-based vibration isolators," *Nonlinear Dyn.*, vol. 99, no. 3, pp. 1823–1839, Feb. 2020, doi: 10.1007/s11071-019-05391-x.
[5] X. Dong, J. Xi, P. Chen, and W. Li, "Magneto-rheological variable inertia flywheel," *Smart Mater. Struct.*, vol. 27, no. 11, p. 115015, Nov. 2018, doi: 10.1088/1361-665X/aad42b.
[6] T. Xu, M. Liang, C. Li, and S. Yang, "Design and analysis of a shock absorber with variable moment of inertia for passive vehicle suspensions," *J. Sound Vib.*, vol. 355, pp. 66–85, Oct. 2015, doi: 10.1016/j.jsv.2015.05.035.
[7] A. C. Mahato, S. K. Ghoshal, and A. K. Samantaray, "Influence of variable inertia flywheel and soft switching on a power hydraulic system," *SN Appl. Sci.*, vol. 1, no. 6, p. 605, Jun. 2019, doi: 10.1007/s42452-019-0623-0.
[8] Y. Zhang, X. Zhang, T. Qian, and R. Hu, "Modeling and simulation of a passive variable inertia flywheel for diesel generator," *Energy Rep.*, vol. 6, pp. 58–68, Dec. 2020, doi: 10.1016/j.egyr.2020.01.001.
[9] D. G. Ullman, "A variable inertia flywheel as an energy storage system," The Ohio State University, 1978.
[10] C. Jauch, "A flywheel in a wind turbine rotor for inertia control," *Wind Energy*, vol. 18, no. 9, pp. 1645–1656, Sep. 2015, doi: 10.1002/we.1784.